Supporting Information for "Subnanometer substructures in nanoassemblies formed from clusters under a reactive atmosphere revealed using machine learning"

Janis Timoshenko[†#]*, *Avik Halder*[‡#], *Bing Yang*[‡], *Soenke Seifert*[‖], *Michael J Pellin*[‡], *Stefan Vajda*[‡^], *Anatoly I. Frenkel*[†,§*]

[†]Department of Materials Science and Chemical Engineering, Stony Brook University, Stony Brook, New York 11794, United States

[‡]Materials Science Division, Argonne National Laboratory, 9700 South Cass Avenue, Argonne, Illinois 60439, United States

[‖]X-ray Science Division, Argonne National Laboratory, 9700 South Cass Avenue, Argonne, Illinois 60439, United States

^ Institute for Molecular Engineering, The University of Chicago, 5640 South Ellis Avenue, Chicago, Illinois 60637, United States

[§]Chemistry Department, Brookhaven National Laboratory, Upton, New York 11973, United States

[#] equally contributing first authors

I. DETAILS OF AB INITIO CALCULATIONS OF XANES

Similarly to our previous works,[1-2] for simulations of Cu K-edge XANES spectra we relied on two state-of-the art *ab initio* codes: FEFF[3] and FDMNES.[4] In both cases the non-structural parameters for XANES simulations were chosen to ensure an as good as possible agreement between the simulated spectrum for bulk copper and experimental Cu foil XANES data.

FEFF version 9.6.4 was used for self-consistent calculations within full multiple scattering (FMS) and muffin-tin (MT) approximations. For nanoparticles FMS cluster size is chosen at a large enough value so that the whole cluster is included in the FMS calculations. We used the default value (1.4 Å) for Cu MT radius, complex exchange–correlation Hedin–Lundqvist potential and random phase approximation (RPA) to model core-hole. For FDMNES calculations we used FDMNES II program (revision 9) and FMS and MT approximations (as in FEFF). For FDMNES calculations we used real Hedin–Lundqvist exchange–correlation potential.

Cluster models for XANES calculations were constructed by cutting with (100) and (111) planes the face-centered cubic structure of bulk copper with lattice constant a_0 =3.615 Å.[5] To model an interface with the support, regular structure models were further truncated with an additional (100) or (111) plane. In addition, icosahedral and hexagonal close-packed clusters were constructed as in Ref.[6] To explore also the sensitivity of XANES data to interatomic distances, we constructed additional structure models by isotropically stretching or compressing the models from the original set, so that the distance between nearest neighbors R changed between 2.2 and 2.6 Å.

Using both FDMNES and FEFF, XANES calculations for all non-equivalent sites in all cluster models were performed. Particle averaged XANES spectra were obtained by averaging corresponding site-specific spectra.[7-8] The obtained spectra were shifted in energy by ΔE to align the energy scale

used in theoretical calculations with the energy scale of experimental data. The values of ΔE (different for FEFF and FDMNES) were chosen so that experimental and calculated Cu K-edge XANES for bulk Cu are aligned. Next, we re-interpolated the theoretical and experimental spectra on a non-uniform mesh that spanned energies from $E_{\min}$ = 8986.9 eV to $E_{\max}$ = 9066.0 eV. Mesh step size was 0.2 eV for data points near the absorption edge, and gradually increased up to 1.0 eV for points at $E = E_{\max}$.

II. DETAILS OF NEURAL NETWORK IMPLEMENTATION AND TRAINING

Similarly to our previous works[1-2, 9], to construct and train neural network (NN) we rely on the off-the-shelf available NN implementation in *Wolfram Mathematica* 11.3.[10] Our NN is a composite function that takes as input discretized XANES spectrum and yields as output a vector that describes relevant structure parameters (coordination numbers (CNs) for the first four coordination shells (C_1, C_2, C_3, C_4) and effective interatomic distance R). NN can be represented as a network of nodes. The output layer of our NN thus contains five nodes, corresponding to the number of output parameters. The number of nodes in the input layer (115) is determined by the number of points in the discretized spectrum. The number of nodes in the intermediate (hidden layers), as well as the number of hidden layers itself are hyperparameters of the NN and are optimized to ensure optimal performance of NN on validation set (see below). In our case we have found that good accuracy can be achieved with two hidden layers with 300 nodes in each.

Each node in the NN adds all its inputs $x^{[n-1](i)}$, weighted with weights $\theta^{[n](i,j)}$. Unit feature $x^{[n-1](0)} = 1$ accounts for the bias term. A non-linear, differentiable activation function f is then applied to the sum, and the output $x^{[n]j} = f\left(\sum_j x^{[i-1]j}\theta^{[n](i,j)}\right)$ is then similarly processed in the

nodes in the consequent NN layers. For hidden layers as activation function we use hyperbolic tangent function, while identity function is used for the output nodes.

To establish relation between the features in averaged XANES $\mu(E)$ and structure parameters $\{C_1, C_2, C_3, C_4, R\}$, and to find the values of NNs weights $\theta^{[n](i,j)}$, we train artificial NN on theoretical XANES data, calculated with FEFF and FDMNES codes for Cu particles of different sizes and shapes and with different interatomic distances. During this procedure, $\theta^{[n](i,j)}$ are iteratively updated so that the difference between NN outputs $\{\tilde{C}_1\ \tilde{C}_2, \tilde{C}_3, \tilde{C}_4, \tilde{R}\}$ and the known true values of structure parameters for the models in the training set $\{C_1, C_2, C_3, C_4, R\}$ is minimized for all training spectra.

To reduce the number of XANES calculations, similarly as in our previous works[1, 11] we use for NN training an artificial dataset, created by linearly combining site-specific theoretical XANES spectra for a small ensemble of 21 particles of different sizes and shapes. For each of the sites we perform both FEFF and FDMNES calculations, resulting in site-specific spectra $\mu(E)$. Sets of site-specific coordination numbers $\{c_1, c_2, c_3, \ \ldots\}$ for each of those sites are known. To construct one training example, we select randomly n of these sites, and create the corresponding average spectrum as $\mu^i(E) = \sum_{j=1}^{n} \mu_j(E)/n$, where $\mu_j(E)$ are site-specific spectra calculated either with FEFF or FDMNES for j-th of the randomly chosen sites. The corresponding average CNs can be obtained as $\{C_1, C_2, C_3, \ \ldots\}^i = \sum_{j=1}^{n}\{c_1, c_2, c_3, \ \ldots\}_j /n$. Note that the selected n sites do not need to correspond to the same particle, but we require that Cu—Cu distance R is the same for all used particles. We repeat this process N_t times to generate as many training examples as required. We have found that a good performance of NN can be achieved with n = 3 and N_t equal to 200,000.

In addition, as previously,[1] instead of using XANES spectra $\mu(E)$ directly, as input for NN we provide $\Delta\mu(E) = \mu(E) - \mu_{bulk}(E)$, where μ_{bulk} is XANES spectrum for bulk material. For theoretical spectra calculated with FDMNES and FEFF $\mu_{bulk}(E)$ is obtained in, correspondingly, FDMNES and FEFF calculations for bulk Cu. For experimental XANES spectra as μ_{bulk} we use experimental XANES for Cu foil.

For NN training we use "Adam" optimization algorithm (stochastic gradient descent with an adaptive learning rate) with default parameters values ($\beta_1 = 0.9$ and $\beta_2 = 0.999$). Batch size was 256; NN training was performed for 100 training rounds. Loss function was defined as the L2-norm between output and target vectors averaged across the batch.

To validate the NN accuracy we used another set of theoretical spectra that were not used for NN training. We compared the structure parameter values, yielded by NN from the corresponding XANES spectra, with the true values of these structure parameters. Importantly, unlike it was for NN training, for the validation of our NN we used particle-averaged XANES spectra, corresponding to realistic Cu NPs of specific size and geometry. To construct validation data set we used structure models that were indirectly used for generation of training data set (as explained above), as well as additional 17 particles of different sizes and shapes. Results of such validation for the first coordination number and interatomic distances are shown in Fig.2 in the main text. Results for the 2nd, 3rd and 4th coordination shells are shown in Supporting Figure S1. The performance of NN on validation data set was also used to find the optimal values for NN hyperparameters: number of hidden nodes and layers, types of activation functions, number of iterations for training, etc, were chosen, so that NN yields as good as possible accuracy of structure parameters for the spectra in the validation data set.

To estimate the error bars of the analysis, we repeated NNs training five times with different sets of training examples. The structure parameter values, reported here and in the main text, correspond to average prediction of all five neural networks. The standard deviation of the predictions by five NNs is used as an estimate for the uncertainty.

III. DETAILS OF GISAXS AND GIXANES EXPERIMENTS

In situ GISAXS and GIXANES measurements were performed at beamline 12-ID-C of the Advanced Photon Source at the Argonne National Laboratory. The experimental setup has previously been reported elsewhere.[12-13] Cu_n clusters were deposited on the oxide supports with a surface coverage of 5% of atomic monolayer equivalent. The cluster-decorated supports were placed in a home-built cell reactor of 40 cm^3 internal volume, equipped with Kapton windows that allow X-ray transmission.[13-14] The reaction gas, composed of 20% CO_2, 60% H_2 and 20% He, was mixed in a gas manifold mixer to maintain a 20 sccm flow. After an initial 2 hour long purge of the reactor with the gas mixture, the samples were heated stepwise from 25 °C up to 375 °C under *in situ* reaction conditions at a constant pressure of 1.25 atm. To maximize the sensitivity of the experiment to the particles on the surface of the support, the X-ray beam was scattered off the sample surface close to the angle of total reflection, i.e., the critical grazing incident angle ($\alpha_c = 0.2°$). An additional advantage of the low incident angle is that a long stripe of the sample surface is illuminated by the X-ray beam, which significantly increases measured signal levels in samples with very low surface coverage. The X-ray absorption near edge structure (XANES) data were collected at Cu K edge (8.987 keV) on a fluorescence detector (Vortex) mounted parallel to the sample surface and perpendicular to the incident beam to minimize background from elastic scattering. The spectra of the Cu metal foil, Cu_2O, CuO, and

$Cu(OH)_2$ bulk standards were collected at the 12-BM beamline of the Advanced Photon Source in transmission mode as reference spectra.

During the processing of the GISAXS data, the two-dimensional X-ray images were analyzed by taking cuts in the q_{xy} direction for information about the particle size in the sample plane, and in the q_z direction for information on particle size in vertical direction. Scattering vectors q are calculated as $q=(4\pi/\lambda)\sin(\theta_f)$ where θ_f is the scattering half angle and λ is the wavelength of the X-rays. The GISAXS images were collected at the energy of 8.9 keV. Using a MATLAB based program the two-dimensional images were processed to obtain one-dimensional intensity profiles (i.e., scattering intensity I as a function of scattering vector q) for horizontal and vertical planes of the sample. Temperature dependencies of horizontal cuts are shown in Fig. S3. Intensity profiles were further analyzed by using the IRENA tool suite to obtain the size distribution of the particles distributed on the support.[15] Modelling II tool was used to fit the GISAXS cuts which employs a combination of unified fit tool and size distribution tool. Examples of GISAXS data fitting are shown in Fig. S4. The obtained particle size distributions are shown in Fig. S5. The size of the smallest resolvable particle is 2 nm. No changes of particle sizes in vertical direction were detected upon temperature increase. The GISAXS data / particle sizes in the horizontal plane are discussed in the main text.

IV. SUPPORTING FIGURES

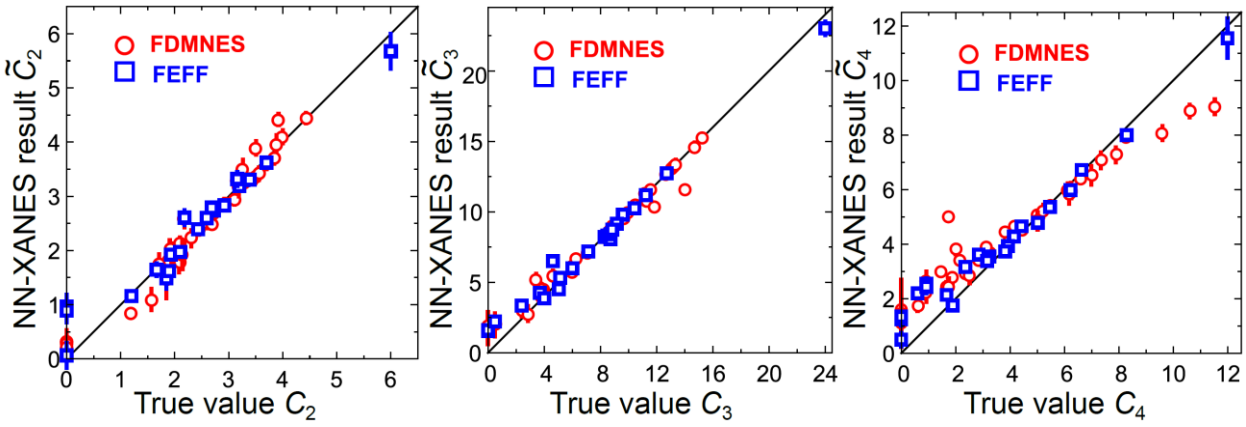

Figure S1. Validation of NN accuracy with theoretical particle-averaged XANES spectra for distant coordination shells. Results of NN-based analysis of theoretical XANES data, obtained in FDMNES[4] and FEFF[3] simulations for Cu particles of different sizes (2nd shell coordination number $\tilde{C}_2$, 3rd shell coordination number $\tilde{C}_3$ and 4th shell coordination number $\tilde{C}_4$) are compared with the true values C_2, C_3 and C_4 for the corresponding particle model.

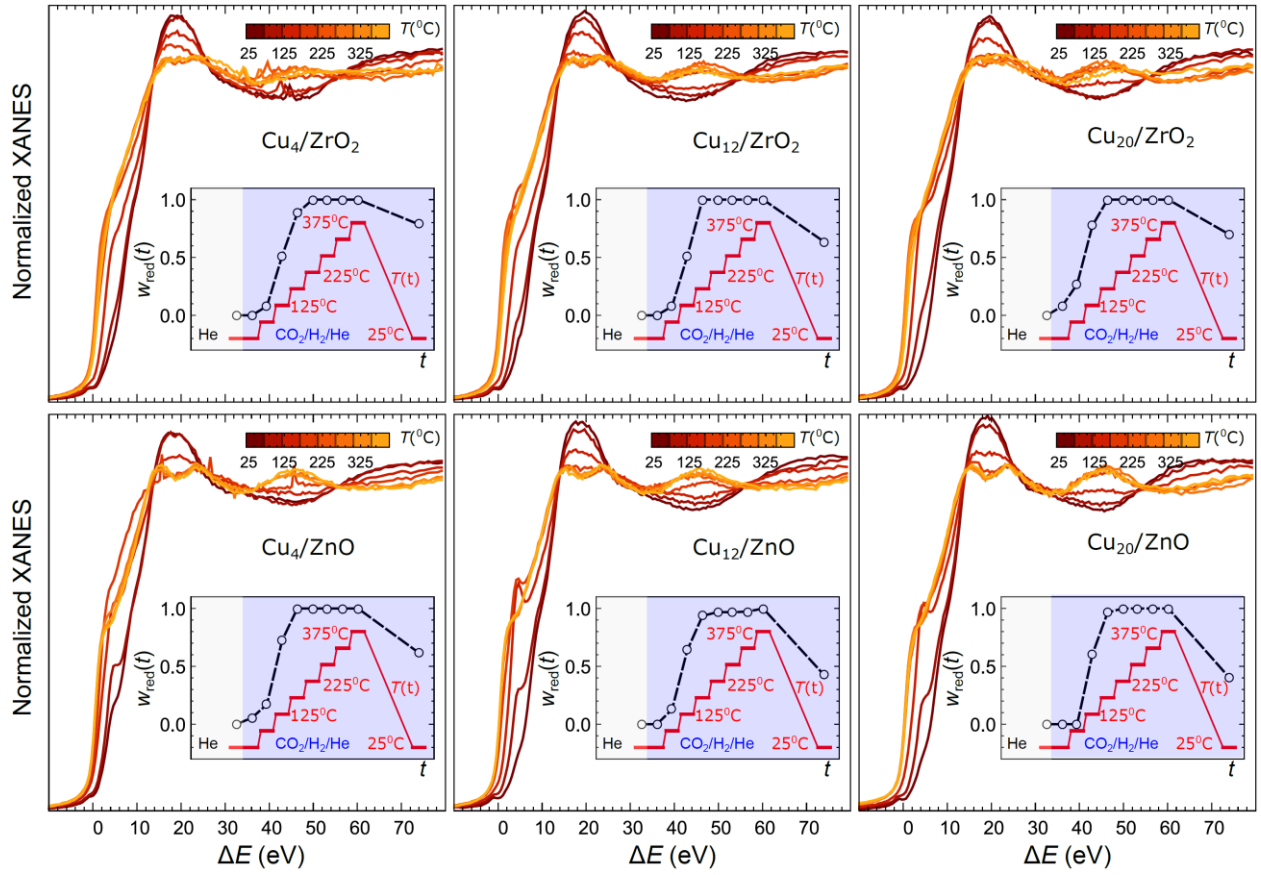

Figure S2. Experimental, temperature-dependent *in situ* XANES for Cu_4, Cu_{12} and Cu_{20} clusters on ZrO_2 and ZnO and temperature-dependencies of the reduced metal fraction w_{red} (see the inset) obtained by linear combination analysis. Applied temperature ramp is also shown in the insets.

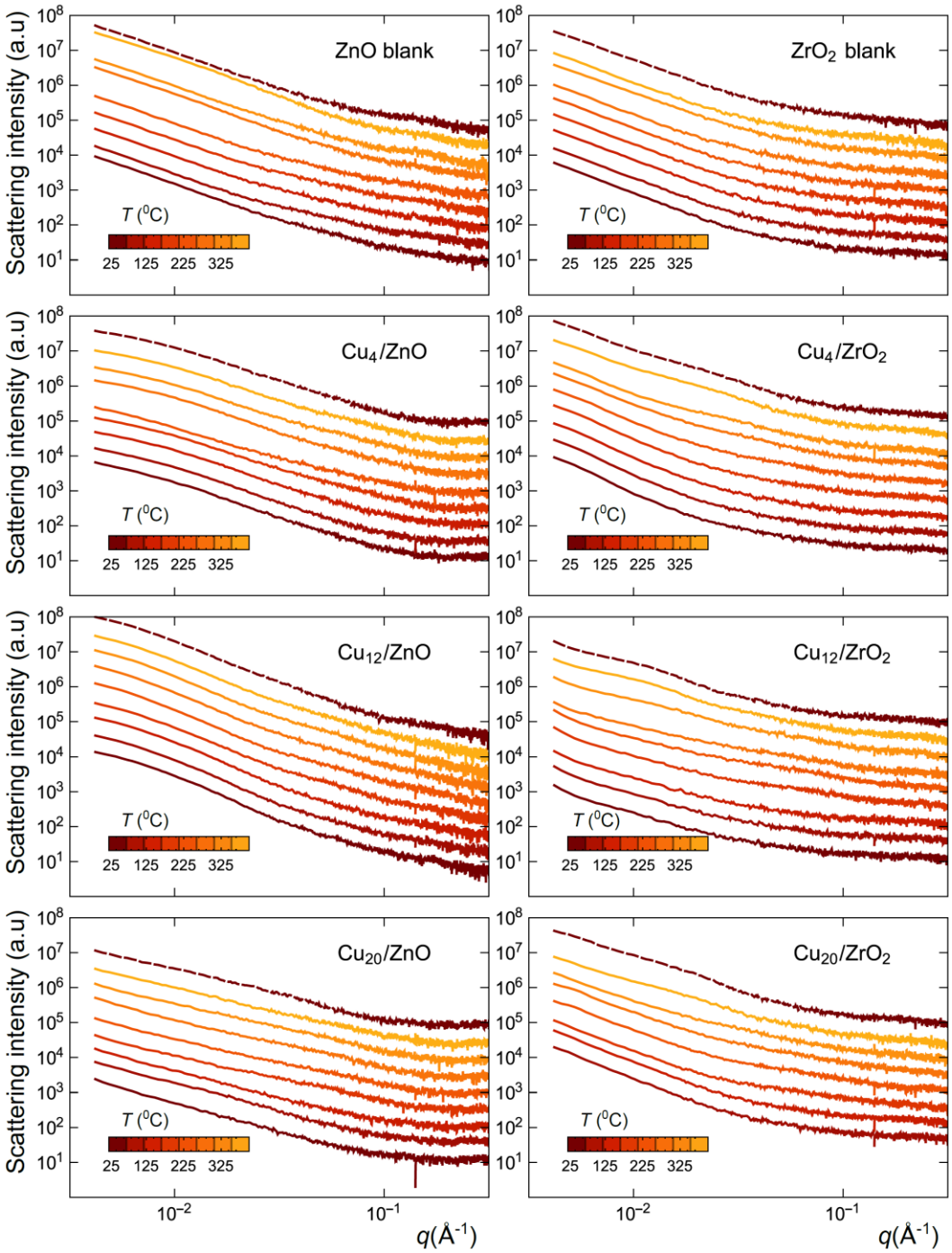

Figure S3: Horizontal cuts of GISAXS data for Cu_4, Cu_{12} and Cu_{20} clusters on ZnO and ZrO_2 supports under the temperature ramp shown in the insets in Fig. S2. For comparison, the horizontal cuts of GISAXS data for oxide supports without clusters deposited are also shown.

The lack of bulge formation in the cuts of GISAXS data confirms that morphology of the support is stable.

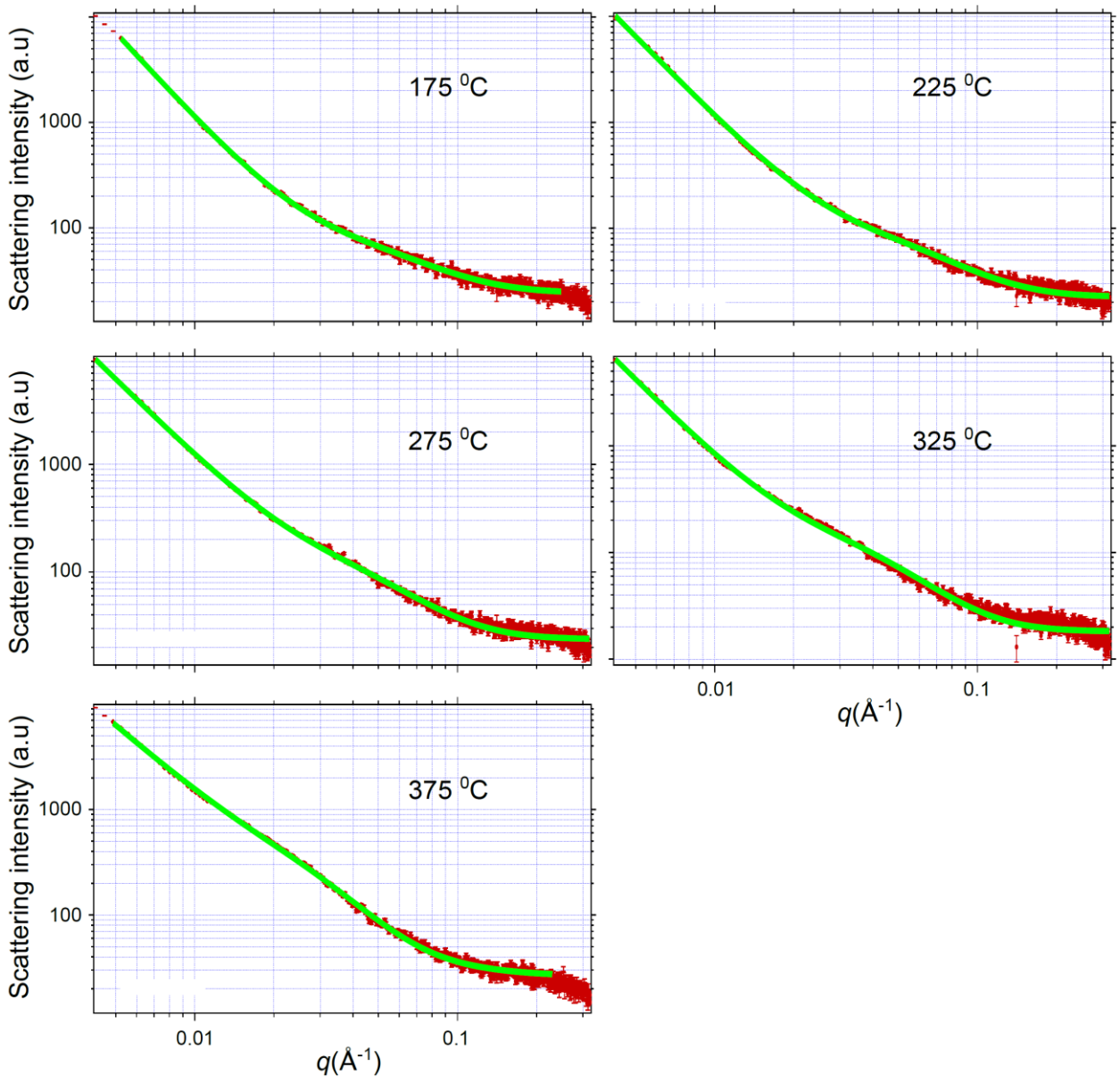

Figure S4: GISAXS data for Cu_4 on ZrO_2 sample (red dots) and fit (green line) obtained by using a log-normal distribution.

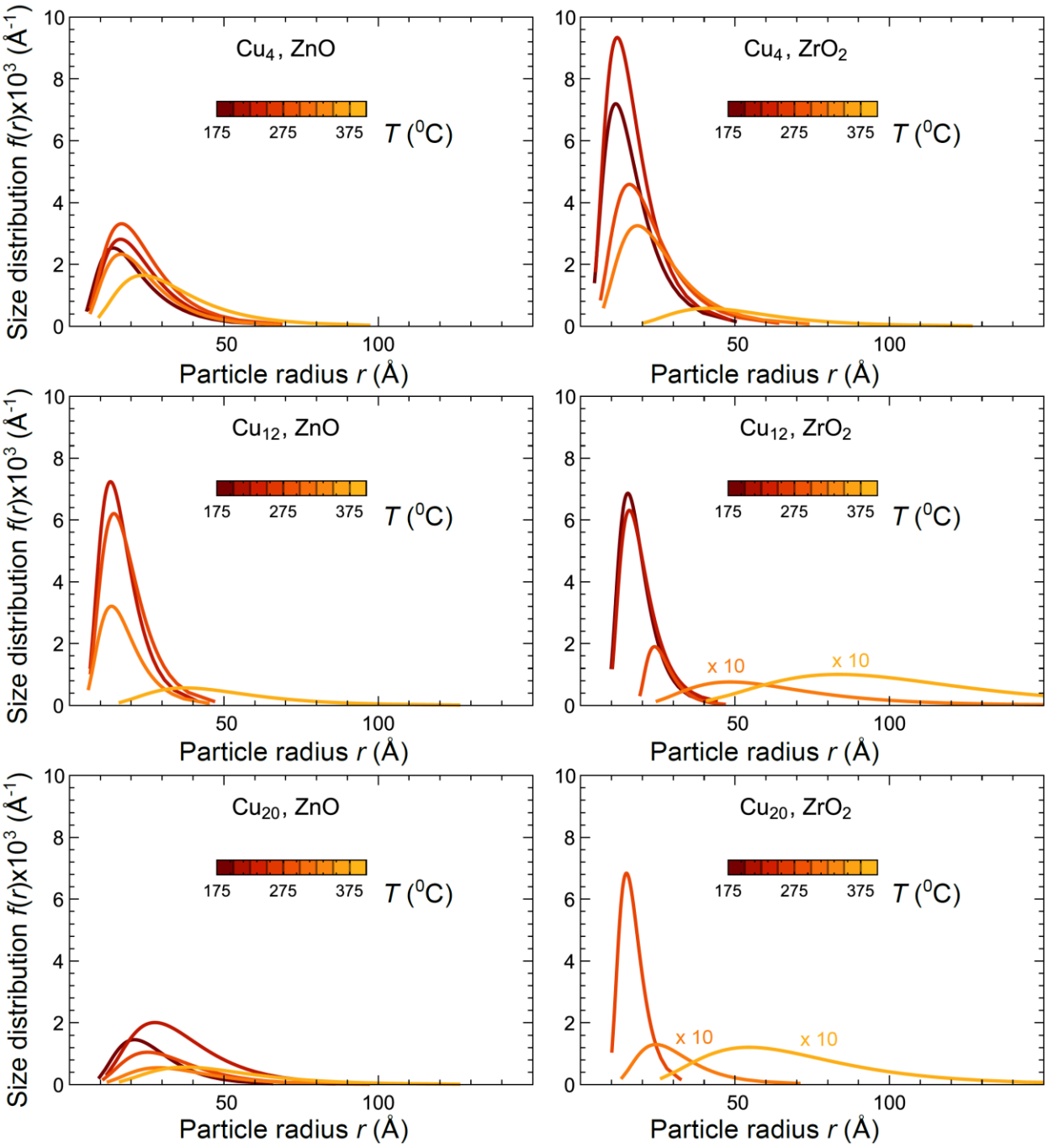

Figure S5: Particle size distributions obtained from GISAXS data for Cu_4, Cu_{12} and Cu_{20} clusters on ZrO_2 and ZnO supports. Results for Cu_{12} and Cu_{20} samples on ZrO_2 at temperatures 225 and 375^{0}C are multiplied by 10 for clarity.

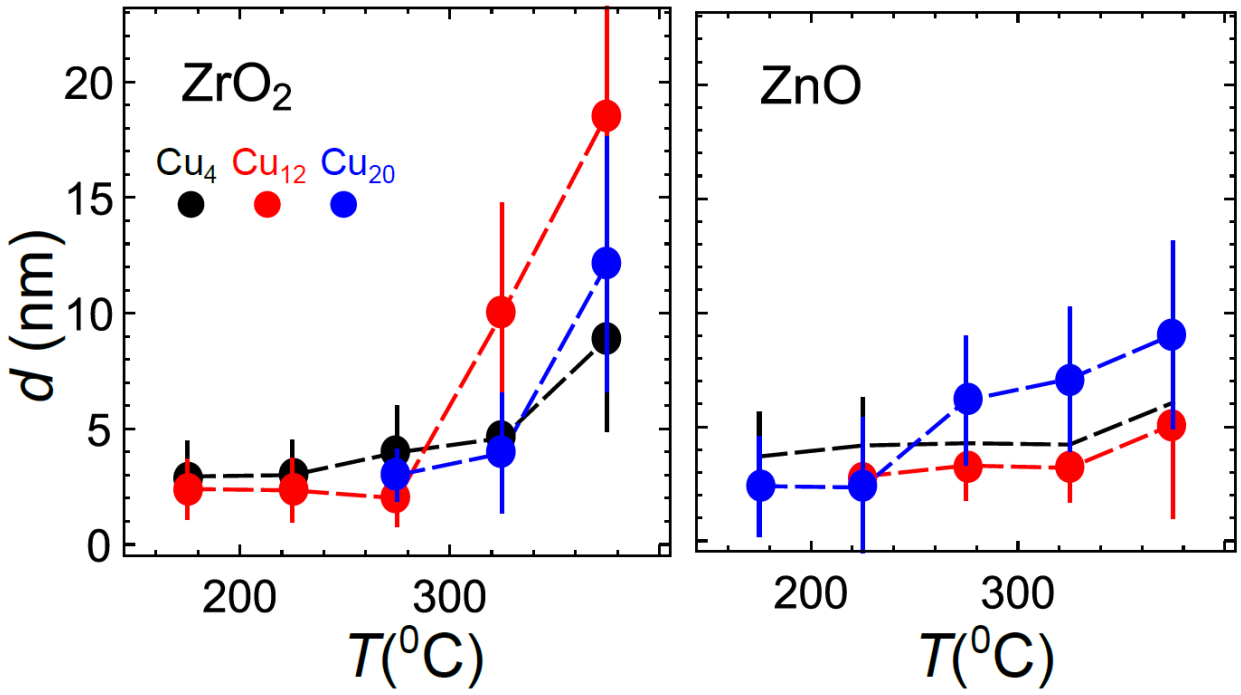

Figure S6: Cluster diameters *d* estimated from GISAXS data for Cu_4, Cu_{12} and Cu_{20} clusters on ZrO_2 and ZnO supports. Dashed lines – guides to the eye. As uncertainties we report here full widths at half maximum for particle size distributions shown in Fig. S5. Note: the smallest resolvable particle size by GISAXS in this experiment is ~ 2 nm. At low temperatures the size of the as-deposited clusters and their assemblies is below the GISAXS detection limit.

AUTHOR INFORMATION

Corresponding Authors

* E-mails: janis.timoshenko@gmail.com, anatoly.frenkel@stonybrook.edu

REFERENCES

1. Timoshenko, J.; Lu, D.; Lin, Y.; Frenkel, A. I., Supervised Machine Learning-Based Determination of Three-Dimensional Structure of Metallic Nanoparticles. *J. Phys. Chem. Lett.* **2017,** *8* (20), 5091-5098.
2. Roese, S.; Kononov, A.; Timoshenko, J.; Frenkel, A. I.; Hövel, H., Cluster Assemblies Produced by Aggregation of Preformed Ag Clusters in Ionic Liquids. *Langmuir* **2018**.

3. Rehr, J. J.; Kas, J. J.; Vila, F. D.; Prange, M. P.; Jorissen, K., Parameter-free calculations of X-ray spectra with FEFF9. *Phys. Chem. Chem. Phys.* **2010,** *12* (21), 5503-5513.
4. Bunău, O.; Joly, Y., Self-consistent aspects of X-ray absorption calculations. *J. Phys.: Condens. Matter* **2009,** *21* (34), 345501.
5. Straumanis, M.; Yu, L., Lattice parameters, densities, expansion coefficients and perfection of structure of Cu and of Cu–In α phase. *Acta Crystallographica Section A: Crystal Physics, Diffraction, Theoretical and General Crystallography* **1969,** *25* (6), 676-682.
6. Glasner, D.; Frenkel, A. I., Geometrical characteristics of regular polyhedra: application to EXAFS studies of nanoclusters. *AIP Conf. Proc.* **2007,** *882* (1), 746-748.
7. Ankudinov, A.; Rehr, J.; Low, J. J.; Bare, S. R., Sensitivity of Pt X-ray absorption near edge structure to the morphology of small Pt clusters. *J. Chem. Phys.* **2002,** *116* (5), 1911-1919.
8. Bazin, D.; Sayers, D.; Rehr, J.; Mottet, C., Numerical simulation of the platinum LIII edge white line relative to nanometer scale clusters. *J. Phys. Chem. B* **1997,** *101* (27), 5332-5336.
9. Timoshenko, J.; Anspoks, A.; Cintins, A.; Kuzmin, A.; Purans, J.; Frenkel, A. I., Neural Network Approach for Characterizing Structural Transformations by X-Ray Absorption Fine Structure Spectroscopy. *Phys Rev Lett* **2018,** *120* (22), 225502.
10. *Mathematica*, Wolfram Research, Inc.: Champaign, Illinois, 2018.
11. Roese, S.; Kononov, A.; Timoshenko, J.; Frenkel, A.; Hoevel, H., Cluster Assemblies Produced by Aggregation of Preformed Ag Clusters in Ionic Liquids. *Langmuir* **2018,** *tbd* (tbd), tbd.
12. Lei, Y.; Mehmood, F.; Lee, S.; Greeley, J.; Lee, B.; Seifert, S.; Winans, R. E.; Elam, J. W.; Meyer, R. J.; Redfern, P. C., Increased silver activity for direct propylene epoxidation via subnanometer size effects. *Science* **2010,** *328* (5975), 224-228.
13. Lee, S.; Lee, B.; Seifert, S.; Vajda, S.; Winans, R. E., Simultaneous measurement of X-ray small angle scattering, absorption and reactivity: A continuous flow catalysis reactor. *Nuclear Instruments and Methods in Physics Research Section A: Accelerators, Spectrometers, Detectors and Associated Equipment* **2011,** *649* (1), 200-203.
14. Vajda, S.; White, M. G., Catalysis Applications of Size-Selected Cluster Deposition. *Acs Catalysis* **2015,** *5* (12), 7152-7176.
15. Ilavsky, J.; Jemian, P. R., Irena: tool suite for modeling and analysis of small-angle scattering. *Journal of Applied Crystallography* **2009,** *42* (2), 347-353.